International Journal of Energy Research

INTERNATIONAL JOURNAL OF ENERGY RESEARCH
Int. J. Energy Res. (2012)
Published online in Wiley Online Library (wileyonlinelibrary.com). DOI: 10.1002/er.2967

Maximum overall efficiency for a solar-driven gas turbine power plant

Susana Sánchez-Orgaz[1], Alejandro Medina[2,*,†] and Antonio Calvo Hernández[2,3]

[1]Departamento de Física, Ingeniería y Radiología Médica, ETSII de Béjar, Universidad de Salamanca, 37700 Béjar, Salamanca, Spain
[2]Departamento de Física Aplicada, Universidad de Salamanca, 37008 Salamanca, Spain
[3]IUFFYM, Universidad de Salamanca, 37008 Salamanca, Spain

SUMMARY

A general model for an irreversible solar-driven Brayton multi-step heat engine is presented. The model incorporates an arbitrary number of turbines (N_t) and compressors (N_c) and the corresponding reheating and intercooling processes; thus, the solar-driven Ericsson cycle is a particular case where $N_t, N_c \to \infty$. For the solar collector, we assume linear heat losses, and for the Brayton multi-step cycle, we consider irreversibilities arising from the non-ideal behavior of turbines and compressors, pressure drops in the heat input and heat release, heat leakage through the plant to the surroundings, and non-ideal couplings of the working fluid with the external heat reservoirs. We obtain the collector temperatures at which maximum overall efficiency $\eta_{\max}$ is reached as a function of the thermal plant pressure ratio, and a detailed comparison for several plant configurations is given. This maximum efficiency is obtained in two cases: when only internal irreversibilities are considered and when both internal and external irreversibilities (which corresponds to the fully irreversible realistic situation) are simultaneously taken into account. Differences between both situations are stressed in detail. In the fully irreversible realistic case, it is possible to perform an additional optimization with respect to the pressure ratio, $\eta^*_{\max}$. In particular, this double optimization leads to a valuable increase in efficiency (between 34% and 65%) for a plant with two turbines and two compressors compared to the simple solar-driven one-turbine one-compressor Brayton engine. Copyright © 2012 John Wiley & Sons, Ltd.

KEY WORDS

thermodynamic optimization; solar-driven heat engines; multi-step gas turbine; irreversibilities; plant performance

Correspondence

*A. Medina, Departamento de Física Aplicada, Universidad de Salamanca, 37008 Salamanca, Spain.
†E-mail: amd385@usal.es

Received 10 February 2012; Revised 28 August 2012; Accepted 30 August 2012

1. INTRODUCTION

Because of energy savings and strategies in minimizing environmental impact, solar-driven heat engines are attracting much interest nowadays, and, as a consequence, different heat engine cycle models coupled to a solar collector have been investigated. Thermodynamic studies analyzing different sources of irreversibilities and different optimization criteria have been reported for solar-driven Carnot [1–7], Ericsson [8,9], Stirling [9,10], and Braysson [11–13] cycles.

In particular, steam, gas, or combined turbine cycles are realistic examples to generate electricity when the heat source is solar energy. Compared to conventional steam turbines, gas turbines have relatively lower thermal efficiencies but bear the advantage of compact building and low construction costs. Moreover, gas turbines can be operated very dynamically (quick start-up) and at significantly lower pressures. The needed heat input can be supplied at least partially (hybrid systems) by concentrating solar collectors using tower plant or dish/engine technology [14–16]. The turbine exhaust energy could be used in a thermal recuperation process through a bottoming cycle [17,18].

In recent years, several prototypes and experimental facilities of solar-driven gas turbine power plants have been developed [19–22]. They usually work on a hybrid solar/fossil fuel operation, so that a standard combustion chamber can compensate for the intermittent nature of solar irradiance. The future commercial interest of this alternative for electric power generation relies on a reduction of investment and generating costs and on an increase of the plant thermal efficiency [23,24]. Theoretical and computer analyses [25–27] on the effect of the main irreversibility sources over the overall thermal efficiency and the optimal values of some basic thermodynamic parameters are necessary steps in order to design efficient solar-driven thermal plants.

Most of the theoretical models devoted to analyze solar-driven gas turbine power plants or solar-driven combined cycle power plants [14,28–30] consider a simple Brayton cycle (with one compressor and one turbine). In principle, a reasonable way to improve cycle performance (which, as previously stated, is nowadays a necessary step for the commercial profitability of these plants) is by incorporating a multi-step compression–expansion procedure with several compressors and turbines. To our knowledge, no theoretical analysis has been fulfilled along this line.

Recently, we have developed a theoretical model [31] for a regenerative multi-step Brayton heat engine (with standard heat input through a combustion chamber) with an arbitrary number of turbines N_t and compressors N_c and incorporating all the irreversibility sources existing in a real plant: the non-ideal behavior of turbines and compressors, pressure drops in the heat input and heat release, regenerator irreversibility, heat leakage through the plant to the surroundings, and non-ideal couplings of the working fluid with the external heat reservoirs. In the present work, we combine the Brayton heat engine model previously developed [31] with a solar collector in such a way that the heat input completely comes from the solar collector. Such combined system offers optimization possibilities completely different that those of its components separately. The analysis of the combined system and its optimization is the main novelty of our work. It is not possible to optimize the efficiency of the solar collector itself with respect to the temperature ratio τ because it is a monotonically decreasing function (losses in the collector increase as it does its working temperature). Conversely, for the conventional Brayton heat engine [32–35], efficiency monotonically increases with the temperature ratio, so it neither admits an optimization. However, the combination of both systems leads to parabolic-shaped efficiency curves when plotted against τ. This fact leads to the existence of a maximum for the combined efficiency and an optimum temperature ratio. We find that such optimum τ corresponds to realistic working temperatures for the solar collector.

Moreover, we shall show that it is feasible to perform simultaneous optimization with respect to the temperature ratio and additionally with respect to the pressure ratio. To our knowledge, this double and simultaneous optimization is presented for the first time. We shall see that the incorporation of a reasonable number of compression–expansion stages and the consideration of optimum pressure and temperature ratios greatly improve the performance of this kind of solar-driven thermal power plants with respect to the simple one-step cycle. This increase reaches 65% for an arrangement with two compressors and two turbines. Our model could be an initial global simulation scheme that would optimize the overall performance records of the plant in terms of a reduced set of parameters (easy to estimate) arising from the irreversibility sources that affect this kind of systems. One of its main advantages is its flexibility because it can be applied to several plant arrangements, independently of the number of compressors and turbines considered and of the details of the solar collector.

The paper is organized as follows. In Section 2, we present the model for the concentrating solar collector and summarize the main characteristics of the multi-step Brayton cycle developed in [31]. In Section 3, we recover some published results in order to show the consistency of the model. In addition, in order to analyze such situations where the number of compressors and turbines is different, we present an analysis of two particular limit cases when the number of turbines and compressors is highly asymmetric: $N_t = 1, N_c \to \infty$ and $N_t \to \infty$, $N_c = 1$. We shall see that there are significant differences between both configurations. In Section 4, we present the general results for the overall efficiency when optimized with respect to the temperature of the solar collector. The obtained results show that it is possible to perform an additional optimization of the overall efficiency with respect to the pressure ratio, which is presented in Section 5. In particular, from such optimization, a significant increase in the efficiency (between 34% and 65%) is predicted for a plant configuration with two turbines and two compressors compared with the basic Brayton solar-driven engine with one compressor and one turbine. Finally, in Section 6, we present a summary and the main conclusions of the work.

2. THEORETICAL MODEL

The configuration scheme and the *T*-*S* diagram of our model for an irreversible solar-driven multi-step Brayton heat engine are depicted in Figure 1. The Brayton heat engine absorbs a net heat rate $|\dot{Q}_H|$ from the solar collector at temperature T_H and releases a net heat rate $|\dot{Q}_L|$ to the ambient at temperature T_L. We also assume a linear heat leakage $|\dot{Q}_{HL}|$ directly from the hot reservoir at T_H to the cold heat sink at T_L [6].

Following Duffie *et al.* [36] and Zhang *et al.* [29], we consider a concentrating collector for which heat losses at low and intermediate temperatures are essentially associated to conduction and convection, whereas at high enough temperatures, radiation losses are dominant. In this model, the useful energy delivered to the heat engine, $|\dot{Q}_H|$, and the efficiency of the solar collector, η_s, can be written, respectively, as

$$|\dot{Q}_H| = \eta_0 G A_a - U_L A_r T_L(\tau - 1), \tag{1}$$

$$\eta_s = \frac{|\dot{Q}_H|}{G A_a} = \eta_0[1 - (\tau - 1)M] \tag{2}$$

In these equations, $\tau = T_H/T_L$ denotes the heat reservoirs temperature ratio; G is the solar irradiance; A_a and A_r are, respectively, the aperture and absorber areas; $C = A_a/A_r$ is the concentration ratio; η_0 is the effective transmittance–absorptance product (optical efficiency); and M is defined as $M = U_L T_L/(\eta_0 G C)$, where U_L is an overall effective coefficient accounting for radiation losses in a linearized heat loss term [29,36]. We have checked that all the results in this work are not affected by the consideration of explicit radiation losses depending on τ^4 (as done, for instance, by Wu *et al.* [13]). The shape of all the figures we shall show is unaltered, and

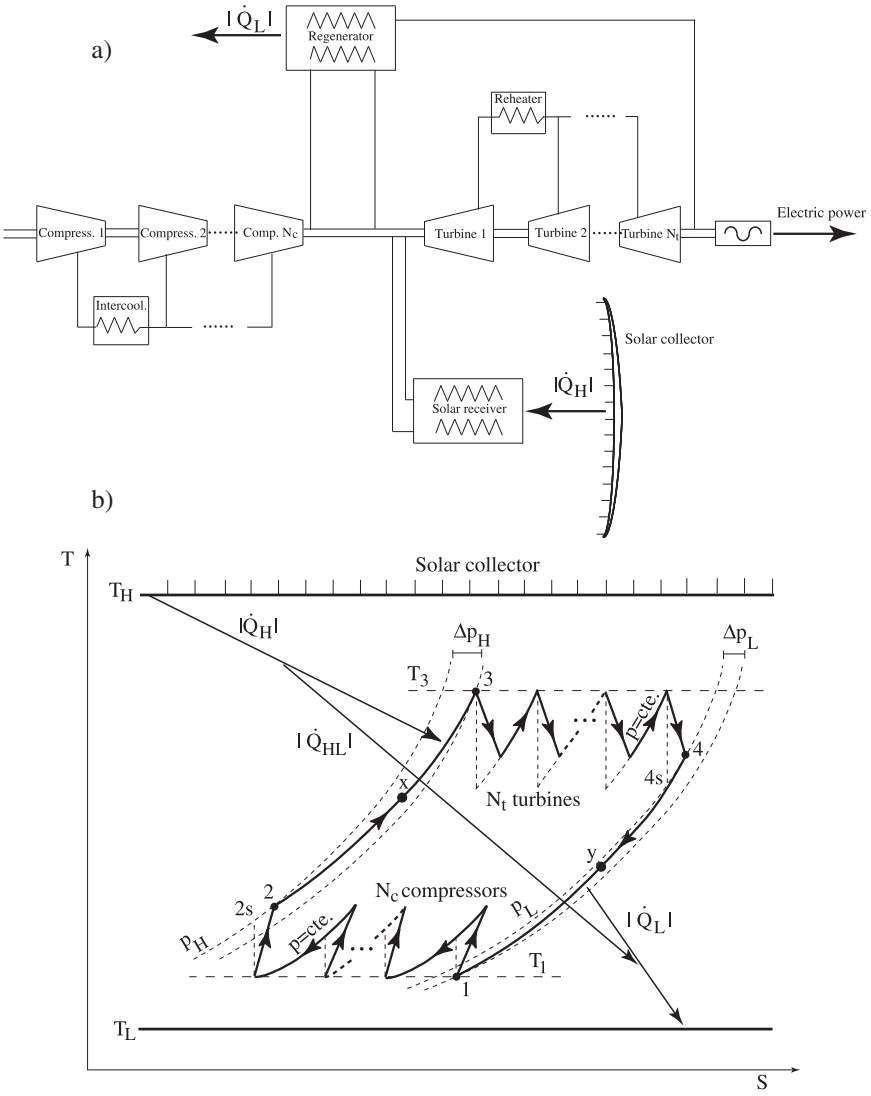

Figure 1. (a) Schematic representation of a solar-powered multi-stage gas turbine plant and (b) *T-S* diagram of our model for a solar-driven multi-step regenerative Brayton cycle.

there are only very small fluctuations on some particular numerical values.

Next, we briefly mention the most important steps in the thermodynamic cycle (see [31] for details):

1. The working fluid, a constant mass flow of an ideal gas with constant heat capacities and adiabatic coefficient γ, is compressed from the initial state 1 by means of N_c non-adiabatic compressors and $N_c - 1$ isobaric intercoolers. All the compressors are assumed to have the same isentropic efficiency ε_c and the same inlet temperature T_1. In a recent study for a solarized Braysson cycle, Wu *et al.* [13] have evaluated the influence of temperature-dependent heat capacities in the overall efficiency. They reported differences below 2% (Table I in [13]) in comparison with the case where the heat capacity remains constant. Thus, in order to obtain analytical expressions for heat input and heat release, we assume constant heat capacities for the working fluid.
2. After state 2, the gas is pre-heated to state X in a regenerative counterflow heat exchanger with effectiveness ε_r. A non-regenerative cycle corresponds to $\varepsilon_r = 0$ whereas ideal or limit regeneration corresponds to $\varepsilon_r = 1$. After X, the working fluid is heated up to the final maximum temperature T_3. The global irreversibilities in this hot-end heat exchanger are accounted by $\varepsilon_H = (T_X - T_3)/(T_X - T_H)$. The overall heating process from state 2 to state 3 is considered as non-isobaric, with a pressure drop quantified by ρ_H [34], which is defined as $\rho_H = (p_3/p_2)^{(\gamma-1)/\gamma} = [(p_H - \Delta p_H)/p_H]^{(\gamma-1)/\gamma}$. Thus, $\rho_H = 1$ corresponds to a zero pressure decay.

Table I. Maximum double optimized efficiency $\eta^*_{\max}$ for the indicated configurations (see text) and the corresponding values of the pressure ratio $r^*_{p,\max}$ and temperature ratio $\tau^*_{\max}$. Results are for the indicated values of external irreversibilities parameters $\varepsilon_H = \varepsilon_L \equiv \varepsilon$. Other parameters used in the computations are as those in Figure 4.

	$\eta^*_{\max}$			$r^*_{p,\max}$			$\tau^*_{\max}$		
ε	0.75	0.90	1	0.75	0.90	1	0.75	0.90	1
CBTX	0.047	0.071	0.086	2.327	2.749	3.102	3.249	3.063	2.972
CBTBTX	0.055	0.081	0.098	2.549	3.143	3.687	3.161	2.986	2.900
CICBTX	0.064	0.087	0.101	2.881	3.406	3.821	3.096	2.956	2.885
CICBTBTX	0.077	0.102	0.116	3.480	4.385	5.177	2.992	2.866	2.802
IT	0.065	0.094	0.112	2.891	3.839	4.864	3.060	2.897	2.817
IC	0.089	0.108	0.119	4.306	4.955	5.429	2.938	2.841	2.792

3. From state 3 to state 4, the working fluid is expanded by means of N_t non-adiabatic turbines and $N_t - 1$ isobaric reheaters. The efficiency of all turbines is the same, ε_t, and the inlet temperature for all of them is T_3.
4. The exhaust process between 4 and 1 splits into two parts: a cooling from 4 to Y through a regenerative heat exchanger with effectiveness ε_r and a subsequent cooling from T_Y to T_1. $\varepsilon_r = 0$ corresponds to $T_Y = T_4$ and $\varepsilon_r = 1$ to $T_Y = T_2$. The effectiveness of this irreversible heat transfer is denoted as $\varepsilon_L = (T_1 - T_Y)/(T_L - T_Y)$. A pressure decay is considered during the whole cooling process, which is quantified by $\rho_L = (p_1/p_4)^{(\gamma-1)/\gamma} = [(p_L - \Delta p_L)/p_L]^{(\gamma-1)/\gamma}$ ($\rho_L = 1$ corresponds to a zero pressure decay in this process) [34].

The basic mathematical equations of the model read as

$$\left|\dot{Q}_H\right| = C_w T_L \left\{ \varepsilon_H \left[\tau - Z_c(1-\varepsilon_r)\frac{T_1}{T_L} - \varepsilon_r Z_t \frac{T_3}{T_L} \right] + \varepsilon_t (N_t - 1)\left(1 - a_t^{-1/N_t}\right)\frac{T_3}{T_L} + \left|\dot{Q}_{HL}\right| \right\} \tag{3}$$

$$\left|\dot{Q}_L\right| = C_w T_L \left\{ \varepsilon_L \left[-1 + Z_t(1-\varepsilon_r)\frac{T_3}{T_L} + \varepsilon_r Z_c \frac{T_1}{T_L} \right] + \frac{1}{\varepsilon_c}(N_c - 1)\left(a_c^{1/N_c} - 1\right)\frac{T_1}{T_L} + \left|\dot{Q}_{HL}\right| \right\} \tag{4}$$

where C_w is the constant heat capacity rate of the working fluid, and

$$Z_c = 1 + \frac{a_c^{1/N_c} - 1}{\varepsilon_c}$$
$$Z_t = 1 - \varepsilon_t\left(1 - a_t^{-1/N_t}\right) \tag{5}$$

$$\frac{T_1}{T_L} = \frac{\varepsilon_L + (1-\varepsilon_L)(1-\varepsilon_r)Z_t\left(\frac{T_3}{T_L}\right)}{1 - (1-\varepsilon_L)\varepsilon_r Z_c} \tag{6}$$

$$\frac{T_3}{T_L} = \frac{\tau\varepsilon_H[1 - (1-\varepsilon_L)\varepsilon_r Z_c] + \varepsilon_L(1-\varepsilon_H)(1-\varepsilon_r)Z_c}{[1 - (1-\varepsilon_L)\varepsilon_r Z_c][1 - (1-\varepsilon_H)\varepsilon_r Z_t] - (1-\varepsilon_H)(1-\varepsilon_L)(1-\varepsilon_r)^2 Z_t Z_c}. \tag{7}$$

In these equations, $a_t = a_c \rho_H \rho_L$, $a_c = T_{2s}/T_1 = r_p^{(\gamma-1)/\gamma}$ is the isentropic compressor pressure ratio and $r_p = P_2/P_1$ is the overall compression ratio. $\left|\dot{Q}_{HL}\right|$ denotes the heat leakage between the heat reservoirs through the plant. It can be expressed as $\xi(\tau - 1)$, where $\xi = C_i/C_w$ is the ratio of the internal conductance of the plant as a whole to that of the working fluid [6,37,38].

Equations (3) and (4) for heat input and heat release, respectively, allow the obtainment of the efficiency of the Brayton heat engine, $\eta_h = \left|\dot{W}\right|/\left|\dot{Q}_H\right| = 1 - \left|\dot{Q}_L\right|/\left|\dot{Q}_H\right|$, where $\left|\dot{W}\right|$ is the net power output of the cycle. This thermal efficiency emerges as a function of the geometrical parameters that characterize the shape and size of the cycle ($\tau = T_H/T_L, r_p, N_c, N_t$), of parameters that quantify the internal irreversibilities (ε_t, ε_c, ρ_H, ρ_L, ε_r, ξ), and of parameters accounting for the external irreversibilities (ε_H,ε_L).

This model for the multi-step Brayton heat engine has been validated and compared with experimental facilities in [39]. Particularly, the predictions of the model for the commercial one-turbine one-compressor regenerative plant Turbec T100 (ABB/Volvo) [40,41] differ by 2.7% for efficiency, 6.7% for the power output, and 4.2% for the heat input. Predicted outputs were also compared with

the experimental ones for a two-compressor one-turbine regenerative plant [42,43]. In this case, the model overestimates experimental efficiency by 2.8% and power output by 1.1%. These results show a fair agreement of our Brayton multi-step theoretical model predictions with real plants.

The efficiency of the overall solar-driven plant $\eta = |\dot{W}|/GA_a$ can be expressed as the product of the efficiencies of the solar collector and of the multi-step Brayton heat engine:

$$\eta = \frac{|\dot{W}|}{GA_a} = \frac{|\dot{W}|}{|\dot{Q}_H|}\frac{|\dot{Q}_H|}{GA_a} \equiv \eta_h \eta_s \tag{8}$$

3. SOME PARTICULAR LIMIT CASES: EXTERNAL IRREVERSIBILITIES

In order to reproduce some particular published results, we shall first analyze the efficiency when only the external irreversibilities associated to the coupling of the thermal system with the external heat reservoirs are considered. This situation is sometimes called *endoreversible* [2,11,12,27,29]; it applies when the engine thermal device behaves as internally reversible, i.e., in practical terms when the main losses arise from the heat exchangers between the working fluid and the solar collector in the hot side and the surroundings in the cold side. In our theoretical scheme, this limit holds when $\varepsilon_L < 1$, $\varepsilon_H < 1$, regeneration is ideal ($\varepsilon_r = 1$), pressure drops in the heat input and heat release are neglected ($\rho_H = \rho_L = 1$), all the turbines and compressors are ideal ($\varepsilon_c = \varepsilon_t = 1$), and heat leakage between reservoirs is not considered ($\xi = 0$). Under these conditions, it is easy to obtain explicit equations for the overall efficiency $\eta = \eta_s \eta_h$, either for a solarized simple Brayton plant ($N_t = N_c = 1$; hereafter B configuration), a solarized Ericsson-like plant ($N_t, N_c \to \infty$; E configuration), and the asymmetric configurations with infinite turbines and one compressor ($N_t \to \infty, N_c = 1$; IT configuration) and one turbine and infinite compressors ($N_t = 1$, $N_c \to \infty$, IC configuration).

For a simple one-turbine one-compressor regenerative plant (B), the overall efficiency is given by

$$\eta = \eta_0[1 - (\tau - 1)M]\left(1 - \frac{k_B}{\tau}\right) \tag{9}$$

with

$$k_B = \left[\frac{(-1 + a + \varepsilon_H)\varepsilon_L}{1 + a(\varepsilon_L - 1)}\right]^{1/2} \tag{10}$$

and

$a = r_p^{(\gamma-1)/\gamma}$. The maximum efficiency (optimized with respect to τ) and the corresponding temperature ratio are given by

$$\eta_{max} = \eta_0\left[(1 + M)^{1/2} - (k_B M)^{1/2}\right]^2 \tag{11}$$

$$\tau_{max} = \left[k_B\left(1 + \frac{1}{M}\right)\right]^{1/2} \tag{12}$$

These results were analyzed by Zhang *et al.* [11,29] in terms of heat transfer coefficients.

In the Ericsson configuration (E), the overall efficiency becomes Carnot's efficiency, so it only depends on the characteristics of the solar collector and τ:

$$\eta = \eta_0[1 - (\tau - 1)M]\left(1 - \frac{1}{\tau}\right) \tag{13}$$

Its maximum and the corresponding temperature ratio are given by

$$\tau_{max} = \left(1 + \frac{1}{M}\right)^{1/2} \tag{14}$$

$$\eta_{max} = \eta_0\left[(1 + M)^{1/2} - M^{1/2}\right]^2 \tag{15}$$

These equations give the performance characteristics of a solar-driven Carnot heat engine with irreversible external couplings. This situation was previously analyzed by different authors [1,7,11,12].

The overall efficiency for the B and E configurations is depicted in Figure 2 for three values of pressure ratios: $r_p = 5$, 15, 20. The following parameters have been selected: $\eta_0 = 0.84$ and $M = 0.29$ for the solar collector [29] and $\varepsilon_H = \varepsilon_L \equiv \varepsilon = 0.90$, $T_L = 300$ K, and $\gamma = 1.4$ for the heat engine [31,32,34,40,44]. From Figure 2, we see that $\eta = \eta(\tau)$ always has a parabolic shape that is independent of r_p for E. We stress that the interval for τ giving positive efficiencies for B rapidly gets narrower for larger pressure ratios. Only for small r_p, the efficiencies for the B arrangement are around 10% or higher.

The existence of a maximum in terms of τ is a consequence of the coupling of the Brayton plant to the solar collector. Efficiency curves for the Brayton plant η_h monotonically increase with the temperature ratio [31], and conversely, for the solar collector, η_s decreases with τ because heat losses increase. Thus, the overall efficiency $\eta = \eta_h \eta_s$ has a parabolic shape and admits an optimization with regard to τ.

In Figure 3(a), we plot the behavior of the optimized efficiencies, $\eta_{max}(r_p)$, and in Figure 3(b), the corresponding temperature ratios, $\tau_{max}(r_p)$: whereas for the E configuration these values are r_p-independent (see Equations (14) and (15)), for the B configuration, $\eta_{max}(r_p)$ ($\tau_{max}(r_p)$) is a decreasing (increasing) function with the pressure ratio, according to Equations (11) and (12), respectively.

Another limit case that allows for an explicit and direct analytical solution is a fully asymmetric configuration with infinite turbines and one compressor (IT) when the only

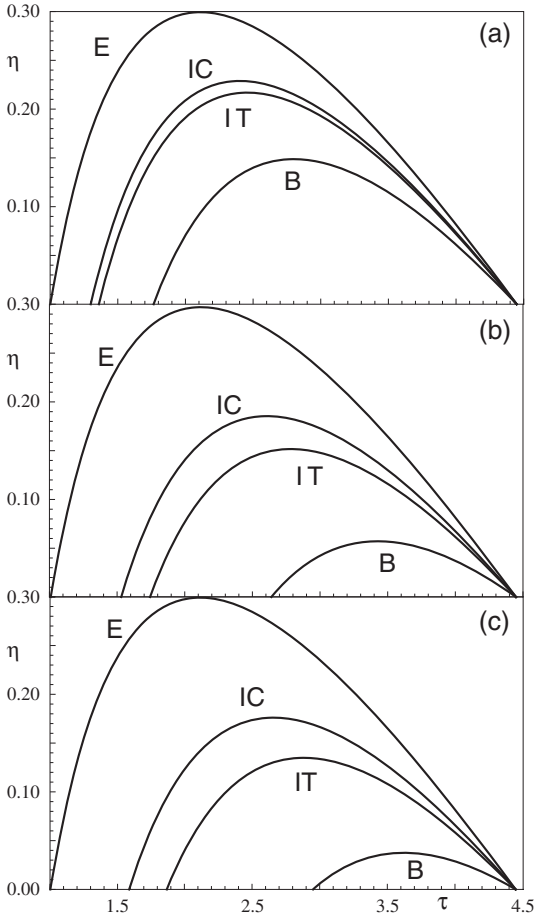

Figure 2. Overall efficiency η of the solar-driven Brayton (B) heat engine, Ericsson (E) and the limits IC ($N_t = 1$, $N_c \to \infty$), and IT ($N_t \to \infty$, $N_c = 1$) as a function of the temperature ratio and at several pressure ratios: (a) $r_p = 5$, (b) $r_p = 15$, and (c) $r_p = 20$. The only irreversibilities arise from the coupling of the heat engine with the external heat reservoirs: $\varepsilon_H = \varepsilon_L \equiv \varepsilon = 0.9$. For the reminder parameters, we take $\eta_0 = 0.84$, $M = 0.29$, $\gamma = 1.4$, $T_L = 300$ K, $\rho_H = \rho_L = 1$, $\varepsilon_t = \varepsilon_c = 1$, $\xi = 0$, and $\varepsilon_r = 1$.

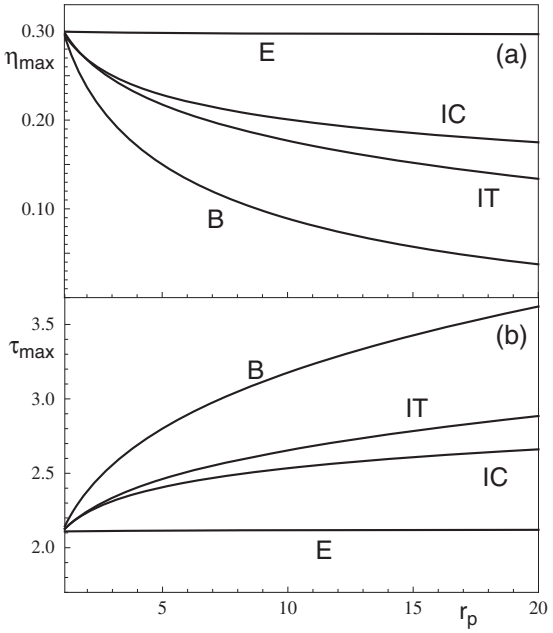

Figure 3. As in Figure 2 but for the (a) maximum overall efficiency η_{max} and (b) the corresponding temperature ratio τ_{max} as functions of the pressure ratio r_p.

irreversibility sources are due to the coupling with the external heat sources. The overall efficiency for this IT arrangement is given by the expression

$$\eta = \eta_0[1 - (\tau - 1)M]\left(1 - \frac{k_{IT}}{\tau}\right) \tag{16}$$

with

$$k_{IT} = \frac{\varepsilon_L(a-1)}{loga[1-(1-\varepsilon_L)a]}. \tag{17}$$

From Equation (16), we obtain the maximum efficiency with respect to τ:

$$\eta_{max} = \eta_0\left[(1+M)^{1/2} - (k_{IT}M)^{1/2}\right]^2 \tag{18}$$

at a temperature ratio τ_{max} given by

$$\tau_{max} = \left[k_{IT}\left(1 + \frac{1}{M}\right)\right]^{1/2} \tag{19}$$

The arrangement with one turbine and infinite compressors (IC) under the same external irreversible conditions also allows for explicit analytical solutions for the overall efficiency and its optimization with respect to the temperature ratio. However, the resulting equations are too intricate, and they are not explicitly reported here.

The behavior of η, η_{max}, and τ_{max} for the IC and IT arrangements are also shown in Figures 2 and 3. From these figures we note that (i) the IC and IT efficiencies are always in between the E and B curves; (ii) the efficiency for IC is greater than IT; (iii) for any value of r_p, the inequality $\eta_{max,E} > \eta_{max,IC} > \eta_{max,IT} > \eta_{max,B}$ holds (Figure 3(a)); and (iv) conversely, temperature ratios at which maximum efficiencies are achieved behave in an opposite way, i.e., $\tau_{max,E} < \tau_{max,IC} < \tau_{max,IT} < \tau_{max,B}$ (Figure 3(b)).

4. FULLY IRREVERSIBLE SYSTEM: OPTIMIZATION WITH RESPECT TO THE TEMPERATURE RATIO

The results in the previous section have been obtained under the so-called endoreversible (or exoirreversible) limit, in which all the accounted irreversibilities come from the couplings between the working system and the external heat reservoirs, whereas the Clausius equality (i.e., reversibility) holds for the cyclic system. These endoreversible models have suffered some criticisms precisely due to the internal reversibility assumption, which is far from most real systems [45–49]. In this sense, the goal of this section is to simultaneously account for all the main irreversibilities affecting the real processes in a solar-powered gas turbine power plant.

We show in Figure 4 the efficiency as a function of τ for the B, E, IT, and IC configurations when both the external and internal irreversibility sources are considered together. We take reference parameters for all the irreversibility sources: $\varepsilon_t = 0.89$, $\varepsilon_c = 0.84$ [44,41,50], $\varepsilon_r = 0.85$ [40,44,50], and $\varepsilon_H = \varepsilon_L$ $\varepsilon = 0.90$ [44], $\rho_H = \rho_L = 0.98$, $\xi = 0.02$, $T_L = 300$ K, and $\gamma = 1.4$ [31,32,34,51]. Parameters for the solar collector are as those in the previous section: $\eta_0 = 0.84$ and $M = 0.29$. From this figure, we mention three relevant facts. First, as in Section 3, Ericsson efficiency is always above IC and IT, and these are, in turn, over the simple regenerative B configuration. This is valid for any value of r_p and τ. Second, and as a consequence of the additional irreversibility sources we consider, the intervals for τ giving positive efficiencies become narrower for the B, IT, and IC configurations as r_p increases. Third, for the r_p values presented ($r_p = 5$, 15, 20), the maximum efficiency for each configuration decreases as r_p increases. Such behavior was also found in the previous section under external irreversibility conditions for all values of the pressure ratio. However, under irreversible conditions, a new and opposite behavior appears when r_p is small enough for all configurations except E: maximum efficiency increases as r_p increases whereas the corresponding τ decreases. This non-monotonic behavior is clearly seen in Figures 5(a) and 5(b), where the differences with plots in Figures 3(a) and 3(b) are substantial, especially on the left-side part.

In Figures 4 and 5, we also show the functions $\eta(\tau)$, $\eta_{\max}(r_p)$, and $\tau_{\max}(r_p)$ for several particular thermal plant arrangements. Following Horlock's notation [52], CICIC...BTBT...X denotes an arrangement where the solar collector is coupled to a thermal plant with several compressors (C) and intermediate intercoolers (I), several turbines (T) and intermediate reheaters (B), and regeneration (X). Thus, CBTX represents a simple Brayton cycle with regeneration, i.e., the so-called B arrangement. Because of economical reasons, plant configurations over two or three turbines or compressors are impractical. From Figure 5(a), we see that at any value of the pressure ratio, the overall optimized efficiency increases in the order B, CBTBTX (one compressor and two turbines), CICBTX (two compressors and one turbine), IT, CICBTBTX (two compressor and two turbines), IC, and E. The opposite

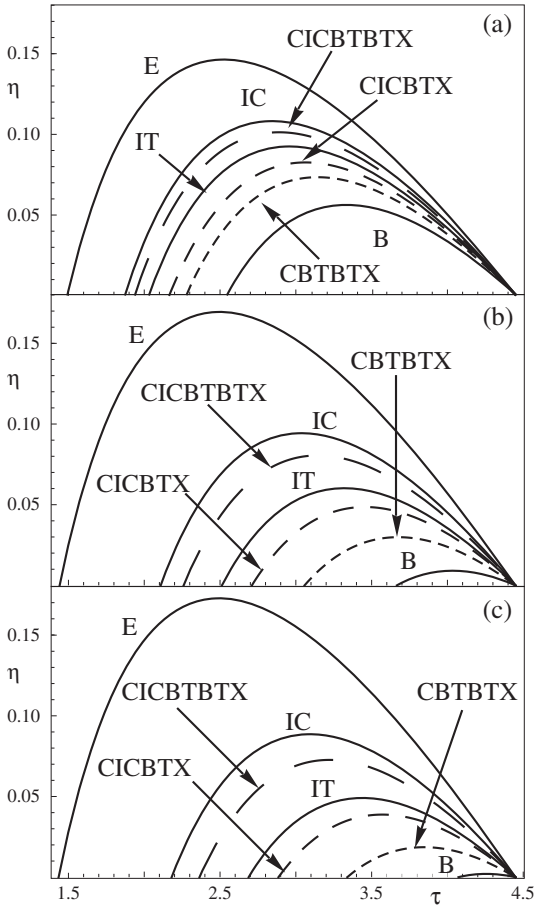

Figure 4. Overall efficiency η for different configurations as a function of the temperature ratio and several pressure ratios: (a) $r_p = 5$, (b) $r_p = 15$, and (c) $r_p = 20$, when both external and internal sources of irreversibilities are taken together: $\eta_0 = 0.84$, $M = 0.29$, $\rho_H = \rho_L = 0.98$, $\varepsilon_t = 0.89$, $\varepsilon_c = 0.84$, $\varepsilon_H = \varepsilon_L \equiv \varepsilon = 0.9$, $\xi = 0.02$, and $\varepsilon_r = 0.85$.

behavior is found for the optimized temperature ratio in Figure 5(b).

The most relevant conclusion from Figure 5(a) is the following: except for E, $\eta_{\max}$ shows a well-defined maximum for small pressure ratio values, whereas at the same pressure ratios, $\tau_{\max}$ shows a minimum. This fact allows an additional optimization of the overall efficiency with respect to r_p, which is presented in the next section. Previously, we analyzed the evolution of the maximum efficiency with M, the parameter that accounts for heat losses of the solar collector. We depict in Figure 6 the evolution of the maximum efficiency and the associated heat reservoir temperature ratio as functions of M, for a particular value of the pressure ratio, $r_p = 15$ (the behavior is similar for other pressure ratios). Figure 6(a) for $\eta_{\max}$ and Figure 6(b) for $\tau_{\max}$ show negative slopes for all the configurations. This is a consequence of the definition of the parameter M. It is proportional to the heat loss in the solar collector, so the larger the heat loss, the lower the operating temperature and the smaller the efficiency of the whole system.

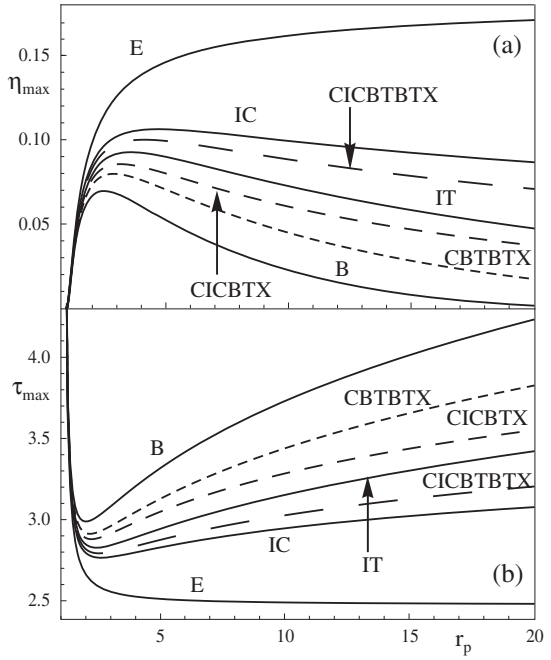

Figure 5. As in Figure 4 but for the (a) maximum overall efficiency η_{max} and (b) the corresponding temperature ratio τ_{max} as functions of the pressure ratio r_p.

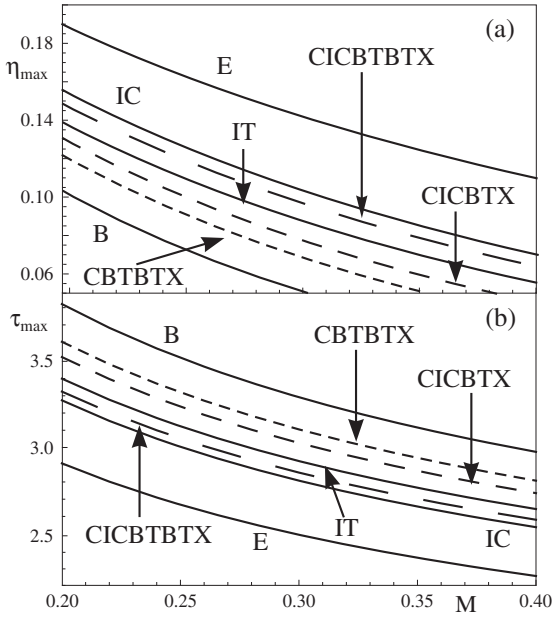

Figure 6. (a) Maximum overall efficiency η_{max} and (b) the corresponding optimum temperature ratio τ_{max} as functions of the parameter M, proportional to the heat losses of the solar collector and $r_p = 5$. Parameters are as those in Figure 4.

Similar results were obtained for solar-driven Carnot [12], Braysson [11–13], and Brayton power plants [29].

5. FULLY IRREVERSIBLE SYSTEM: SIMULTANEOUS OPTIMIZATION WITH RESPECT TO THE PRESSURE AND TEMPERATURE RATIOS

As noted before, the behavior of $\eta_{max}(r_p)$ in the fully irreversible situation (Figure 5(a)) clearly shows that it is possible to maximize again the overall efficiency with respect to r_p. This is not possible when only external irreversibilities are considered, because the curves $\eta_{max}(r_p)$ do not admit maximization in that case (Figure 3(a)). The resulting values after double optimization in the fully irreversible case will be denoted by η^*_{max} and by $r^*_{p,max}$ for the corresponding pressure ratio. We collect in Table I the numerical values of the double optimized efficiency together with the corresponding values of the temperature and pressure ratios. Values presented in the table cover a realistic interval of the effectiveness of the heat exchangers that couple the heat engine with the solar collector and the cold reservoir, from $\varepsilon_H = \varepsilon_L \equiv \varepsilon = 0.75$ to the ideal limit case, $\varepsilon = 1$. Other parameters are those detailed at the beginning of Section 4. From Table I, we stress that

1. The numerical values of optimized efficiency are relatively low, but we should remark that this is a pure solar-driven plant, so there are no operation costs associated to fuel consumption.
2. When all irreversibility parameters are fixed, η^*_{max} and $r^*_{p,max}$ increase compared to B when we consider configurations with two turbines (CBTBTX), two compressors (CICBTX), and two compressors together with two turbines (CICBTBTX). The opposite behavior is found for the corresponding τ^*_{max}; thus, an increase in the number of compressor and/or turbines requires lower optimal temperature in the solar collector and higher pressure ratios.
3. In Table II, we summarize the relative differences of the parameters in Table I when the basic configuration CBTX is compared with the other plant arrangements. The relative differences are very significant. When comparing, for instance, the simplest arrangement CBTX with a configuration with two turbines and two compressors, CICBTBTX, the double-optimized efficiency approximately increases by 34% for $\varepsilon = 1$, 44% for $\varepsilon = 0.9$, and 65% for $\varepsilon = 0.75$. For the corresponding temperature ratio, we have relative decreases of 6.0% for $\varepsilon = 1$, 6.4% for $\varepsilon = 0.9$ and 7.9% for $\varepsilon = 0.75$.

Optimized temperature ratios in Table I for the four realistic configurations are in the interval (2.802, 3.249), which for $T_L = 300$ K gives optimized temperature in the solar collector between 841 K and 975 K. These temperatures can be reached by real power tower and dish/engine systems [15,16].

Although our study intends to be theoretical and predictive, the comparison of the calculated efficiencies with that of prototype plants would be straightforward with the

Table II. Relative variations of the maximized efficiency $\eta^*_{\max}$ and the optimum values for the pressure ratio $r^*_{p,\max}$ and the temperature ratio $\tau^*_{\max}$ for different plant configurations with reference to the basic configuration CBTX.

	$\Delta\eta^*_{\max}$ (%)			$\Delta r^*_{p,\max}$ (%)			$\Delta\tau^*_{\max}$(%)		
ε	0.75	0.90	1	0.75	0.90	1	0.75	0.90	1
CBTBTX	17.8	14.5	13.2	9.5	14.3	18.9	–2.70	–2.51	–2.42
CICBTX	38.3	22.7	16.9	23.8	23.9	23.2	–4.70	–3.49	–2.93
CICBTBTX	64.9	43.7	34.3	49.5	59.5	66.8	–7.90	–6.43	–5.72

knowledge of some basic parameters like the working temperature of the solar collector, its losses, and the size and the basic characteristics of the heat engine: pressure ratio, efficiencies of the regenerator, turbines and compressors, pressure drops, and efficiencies of the heat exchangers. Unfortunately, the complete set of parameters for the experimental facilities built up to now [19,22,53–55] is not available in the literature, so a precise numerical comparison is unfeasible.

6. SUMMARY AND CONCLUSIONS

A thermodynamic analysis for an irreversible solar-driven multi-step Brayton heat engine has been developed. Our model could be used as an *a priori* global simulation scheme in order to foresee the overall plant efficiency as a function of a reduced set of parameters with a direct thermodynamic meaning. We have assumed a solar concentrating collector with heat losses accounted through a linear term proportional to an overall effective heat loss coefficient (and checked that all the results reported are insensitive to an explicit radiation losses term). The irreversible thermodynamic cycle model incorporates the possibility of an arbitrary number of turbines N_t and compressors N_c with the associated reheating and intercooling processes. The overall efficiency of the combined system has been obtained in terms of parameters accounting for both external and internal irreversibility sources.

We have analyzed the optimized overall efficiencies with respect to the temperature ratio $\eta_{\max}$ and the optimum temperature ratio $\tau_{\max}$ for arrangements with different numbers of compressors and turbines. Besides, the overall efficiency admits a double and simultaneous optimization with respect to the pressure ratio r_p and τ, denoted as $\eta^*_{\max}$. For instance, a configuration with two turbines and two compressors (CICBTBTX) is capable of increasing the overall efficiency of the simple regenerative Brayton (CBTX) when optimized simultaneously with respect to r_p and τ between 34% and 65% (Table II), requiring a lower working temperature for the solar collector. The resulting optimized temperatures for the solar collector can be reached by the use of adequate tower plant or parabolic dish/engine technology. The obtained theoretical findings could guide the design and evaluation of advanced solar powered turbine systems beyond the basic one-turbine one-compressor regenerative Brayton cycle [54,55].

As future work lines, we should emphasize the importance of two key components in solar-powered gas turbine plants: the regenerator and the heat exchangers coupling the Brayton thermal engine with the solar collector and with the surroundings. It is well known that for a standard gas turbine, the regeneration effectiveness ε_r is a basic parameter in order to reduce the input heat transfer rate and improve efficiency [31,32,34]. The results we have presented have been obtained for a fixed ε_r, but its influence when the Brayton cycle is coupled to a solar collector probably deserves a deeper analysis. Recent technological developments suggest the importance of the irreversibilities associated with the heat exchangers in the final overall efficiency of the plant [21,40,44,55]. This is another open subject to be investigated in future theoretical works, which probably should include the optimization of some thermoeconomical figure of merit [56,57]. Finally, we remark that our model is capable of accounting for the intermittency of the solar irradiance associated to seasonality, weather conditions, or other effects. Moreover, it is possible to incorporate a standard combustion chamber as it is done in real prototypes in order to avoid fluctuations in the power output.

NOMENCLATURE

A_a	= aperture area of the collector
A_r	= absorber area of the collector
a_c	= isentropic compressor pressure ratio
a_t	= isentropic turbine pressure ratio
C	= concentration ratio
C_i	= internal conductance of the power plant
C_w	= heat capacity rate of the working fluid
CICIC...BTBT...X	= notation for multi-step plant arrangements
IC	= infinite-compressors one-turbine regenerative plant configuration
IT	= infinite-turbines one-compressor regenerative plant configuration
G	= solar irradiance
$\dot{m}$	= mass flow rate of the working substance
M	= loss coefficient for the solar collector
N_c	= number of compressors

N_t = number of turbines
$|\dot{Q}_L|$ = heat transfer rate between the working fluid and the heat reservoir at T_L
$|\dot{Q}_H|$ = heat transfer rate between the working fluid and the heat reservoir at T_H
$|\dot{Q}_{HL}|$ = heat leakage between the heat reservoirs through the plant
r_p = overall pressure ratio
$r^*_{p,\max}$ = optimum pressure ratio after double optimization
T_L = ambient temperature
T_H = temperature of the solar collector
U_L = overall heat loss coefficient of the solar collector
η = overall efficiency
$\eta_{\max}$ = maximum overall efficiency with respect to the temperature ratio
$\eta^*_{\max}$ = maximum overall efficiency with respect to pressure and temperature ratios
η_s = efficiency of the solar collector
η_h = thermal efficiency of the heat engine
η_0 = effective transmittance–absorptance product
ε_c = isentropic efficiency of the compressors
ε_r = regenerator effectiveness
ε_t = isentropic efficiency of the turbines
ε_L = irreversibilities in the coupling of the working fluid with the heat reservoir at temperature T_L
ε_H = irreversibilities in the coupling of the working fluid with the heat reservoir at temperature T_H
ε = external irreversibilities parameter when $\varepsilon_H = \varepsilon_L$
γ = adiabatic coefficient
ρ_L = pressure drop in the heat release process
ρ_H = pressure drop in the heat input process
T = heat reservoirs temperature ratio
$\tau_{\max}$ = optimum temperature ratio
$\tau^*_{\max}$ = optimum temperature ratio after double optimization
ξ = ratio between the heat conductances of the plant and the working fluid
$\Delta\eta^*_{\max}$ = relative variations of $\eta^*_{\max}$ with respect to the basic regenerative plant configuration
$\Delta r^*_{p,\max}$ = relative variations of $r^*_{p,\max}$ with respect to the basic regenerative plant configuration
$\Delta\tau^*_{\max}$ = relative variations of $\tau^*_{\max}$ with respect to the basic regenerative plant configuration

ACKNOWLEDGEMENTS

We acknowledge financial support from MICINN (Spain) under Grant FIS2010-17147.

REFERENCES

1. Gordon JM. On optimized solar-driven heat engines. *Solar Energy* 1988; **40**:457–461.
2. Sahin AZ. Optimum operating conditions of solar-driven heat engines. *Energy Conversation and Management* 2000; **41**:1335–1343.
3. Koyun A. Performance analysis of a solar-driven heat engine with external irreversibilities under maximum power and power density condition. *Energy Conversation and Management* 2004; **45**:1941–1947.
4. Sogut OS, Durmayaz A. Performance optimization of a solar-driven heat engine with finite-rate heat transfer. *Renewable Energy* 2005; **30**:1329–1344.
5. Yilmaz T, Ust Y, Erdil A. Optimum operating conditions of irreversible solar driven heat engines. *Renewable Energy* 2006; **31**:1333–1342.
6. Ust Y. Effects of combined heat transfer on the thermo-economic performance of irreversible solar-driven heat engines. *Renewable Energy* 2007; **32**:2085–2095.
7. Barranco-Jiménez MA, Sánchez-Salas N. On thermodynamic optimisation of solar collector model under maximum ecological conditions. *Journal of the Energy Institute* 2008; **81**:164–167.
8. Blank DA, Wu C. Finite-time power limit for solar-radiant Ericsson engines in space applications. *Applied Thermal Engineering* 1998; **18**:1347–1357.
9. Bädescu V. Optimum operation of a solar converter in combination with a Stirling or Ericsson heat engine. *Energy* 1992; **17**:601–607.
10. Chen J, Yan Z, Chen L, Andresen B. Efficiency bound of a solar driven stirling heat engine system. *International Journal of Energy Research* 1998; **22**:805–812.
11. Zhang Y, Lin B, Chen J. The unified cycle model of a class of solar-driven heat engines and their optimum performance characteristics. *Journal of Applied Physics* 2005; **97**:084905.
12. Zheng S, Chen J, Lin G. Performance characteristics of an irreversible solar-driven Braysson heat engine at maximun efficiency. *Renewable Energy* 2005; **30**:601–610.
13. Wu L, Lin G, Chen J. Parametric optimization of a solar-driven Braysson heat engine with variable heat

capacity of the working fluid and radiation-convection heat losses. *Renewable Energy* 2010; **35**:95–100.
14. Fraidenraich N, Gordon JM, Tiba C. Optimization of gas-turbine combined cycles for solar energy and alternative-fuel power generation. *Solar Energy* 1992; **48**:301–307.
15. Pitz-Paal R. High Temperature Solar Concentrators. In *Solar Energy Conversion and Photoenergy Systems*. UNESCO: Eolss Publishers, 2007.
16. Fernández-García A, Zarza E, Valenzuela L, Pérez M. Parabolic-trough solar collectors and their applications. *Renewable and Sustainable Energy Reviews* 2010; **14**:1695–1721.
17. Ghazikhani M, Passandideh-Fard M, Mousavi M. Two new high-performance cycles for gas turbine with air bottoming. *Energy* 2011; **36**:294–304.
18. Ahmed MS, Mohamed HA. Performance characteristics of modified gas turbine cycles with steam injection after combustion exit. *International Journal of Energy Research* 2011. DOI: 10.1002/er.1916
19. SOLGATE. Solar hybrid gas turbine electric power system. Technical Report EUR 21615, European Commission, 2005.
20. Sinai J, Sugarmen C, Fisher U. Adaptation and modification of gas turbines for solar energy applications. In *Proceedings of GT2005 ASME Turbo Expo 2005*, 2005.
21. Ávila-Marín AL. Volumetric receivers in solar thermal power plants with centra receiver system technology: a review. *Solar Energy* 2011; **85**:891–910.
22. Chacartegui R, Muñoz de Escalona JM, Sánchez D, Monje B, Sánchez T. Alternative cycles based on carbon dioxide for central receiver solar power. *Applied Thermal Engineering* 2011; **31**:872–879.
23. le Roux WG, Bello-Ochende T, Meyer JP. Operating conditions of an open and direct solar thermal Brayton cycle with optimised cavity receiver and recuperator. *Energy* 2011; **36**:6027–6036.
24. Vecchiarelli J, Kawall JG, Wallace JS. Analysis of a concept for increasing the efficiency of a Brayton cycle via isothermal heat addition. *International Journal of Energy Research* 1997; **2**(2):113–127.
25. le Roux WG, Bello-Ochende T, Meyer JP. Thermodynamic optimisation of the integrated design of a small-scale solar thermal brayton cycle. *International Journal of Energy Research* 2012; **36**:1088–1104.
26. Lee JJ, Kang DW, Kim TS. Development of a gas turbine performance analysis program and its application. *Energy* 2011; **36**:5274–5285.
27. Cheng CY, Chen CK. Maximum power of an endoreversible intercooled Brayton cycle. *International Journal of Energy Research* 2000; **24**:485–494.
28. Gandhidasan P. Thermodynamic analysis of a closed--cycle, solar gas-turbine plant. *Energy Conversation and Management* 1993; **34**:657–661.
29. Zhang Y, Lin B, Chen J. Optimum performance characteristics off an irrversible solar-driven Brayton heat engine at the maximum overall efficiency. *Renewable Energy* 2007; **32**:856–867.
30. Baghernejad A, Yaghoubi M. Exergy analysis of an integrated solar combined cycle system. *Renewable Energy* 2010; **35**:2157–2164.
31. Sánchez-Orgaz S, Medina A, Calvo Hernández A. Thermodynamic model and optimization of a multi-step irreversible Brayton cycle. *Energy Conversation and Management* 2010; **51**:2134–2143.
32. Calvo Hernández A, Roco JMM, Medina A. Power and efficiency in a regenerative gas-turbine with multiple reheating and intercooling stages. *Journal of Physics D: Applied Physics* 1996; **29**:1462–1468.
33. Wu C, Chen L, Sun F. Performance of a regenerative Brayton heat engine. *Energy* 1996; **21**:71–76.
34. Roco JMM, Velasco S, Medina A, Calvo Hernández A. Optimum performance of a regenerative Brayton thermal cycle. *Journal of Applied Physics* 1997; **82**:2735–2741.
35. Medina A, Roco JMM, Calvo Hernández A. Regenerative gas turbines at maximum power density conditions. *Journal of Physics D: Applied Physics* 1996; **29**:2802–2805.
36. Duffie JA, Beckman WA. *Solar Engineering of Thermal Processes*. John Wiley and Sons: Hoboken, New Jersey, 2006.
37. Bejan A. *Advanced Engineering Thermodynamics* (3rd edition). Wiley: Hoboken, New Jersey, 2006.
38. Ust Y, Sahin B, Kodal A, Akcay IH. Ecological coefficient of performance analysis and optimization of an irreversible regenerative-Brayton heat engine. *Applied Energy* 2006; **83**:558–572.
39. Sánchez-Orgaz S. Modelization, analysis, and thermodynamic optimization of Brayton multi-step power plants. Solar applications. PhD thesis, Universidad de Salamanca, Spain, 2012.
40. Sunden B. High temperature heat exchangers (HTHE). In *Proceedings of the Fifth International Conference on Enhanced, Compact and Ultra-Compact Heat Exchangers: Science, Engineering and Technology*, Hoboken, NJ, USA, 2005.
41. Kautz M, Hansen U. The externally fired gas turbine (EFGT-cycle) and simulation of the key components. *Applied Energy* 2007; **84**:795–805.
42. Romier A. Small gas turbine technology. *Applied Thermal Engineering* 2004; **24**:1709–1723.
43. EU Project. Coordinator: Microturbo S.A. (France). Research and development of high efficiency components for an intercooled, recuperated CHP gas turbine for combined heat and efficient power. Technical report, Comunidad Europea, Contract No. ENK5-CT-2000-00070, 2000–2003.

44. de Mello PEB, Monteiro DB. Thermodynamic study of an EFGT (externally fired gas-turbine) cycle with one detailed model for the ceramic heat exchanger. In *Proceedings of ECOS 2011 Conference*, Novi Sad, Serbia, 2011.
45. Moran MJ. On second-law analysis and the failed promise of finite-time thermodynamics. *Energy* 1998; **23**:517–519.
46. Sekulic DP. A fallacious argument in the finite time thermodynamic concept of endoreversibility. *Journal of Applied Physics* 1998; **83**:4561–4565.
47. Gyftopoulos EP. Infinite time (reversible) versus finite time (irreversible) thermodynamics: a misconceived distinction. *Energy* 1999; **24**:1035–1039.
48. Ishida M. The role and limitations of endoreversible thermodynamics. *Energy* 1999; **24**:1009–1014.
49. Andresen B. Comment on "A fallacious argument in the finite time thermodynamic concept of endoreversibility". *Journal of Applied Physics* 2001; **90**:6557–6559.
50. Galanti L, Massardo AF. Micro gas turbine thermodynamic and economic analysis up to 500 kWe. *Applied Energy* 2011; **88**:4795–4802.
51. Calvo Hernández A, Medina A, Roco JMM. Power and efficiency in a regenerative gas turbine. *Journal of Physics D: Applied Physics* 1995; **28**:2020–2023.
52. Horlock JH. *Advanced Gas Turbine Cycles*. Pergamon: Oxford, 2003.
53. Gallup DR, Kesseli JB. A solarized Brayton engine based on turbo-charger technology and the DLR receiver. In *Proceedings of the IECEC-AIAA-94-3945*, Monterrey, CA, 1994.
54. Schwarzbözl P, Buck R, Sugarmen C, Ring A, Marcos Crespo MJ, Altwegg P, Enrile J. Solar gas turbine systems: design, cost and perspectives. *Solar Energy* 2006; **80**:1231–1240.
55. Heller P, Pfänder M, Denk T, Tellez F, Valverde A, Fernandez J, Ring A. Test and evaluation of a solar powered gas turbine system. *Solar Energy* 2006; **80**:1225–1230.
56. Spelling J, Favrat D, Martin A, Augsburger G. Thermoeconomic optimization of a combined-cycle solar tower plant. *Energy* 2012; **41**:113–120.
57. Bracco S, Siri S. Exergetic optimization of single level combined gas-steam power plants considering different objective functions. *Energy* 2010; **35**:5365–5373.